

Fingerprint formation

Michael Kücken^{a,*}, Alan C. Newell^{a,b}

^aProgram in Applied Mathematics, University of Arizona, Tucson, AZ 85721, USA

^bDepartment of Mathematics, University of Arizona, Tucson, AZ 85721, USA

Received 17 October 2004; accepted 17 December 2004

Available online 25 February 2005

Abstract

Fingerprints (epidermal ridges) have been used as a means of identifications for more than 2000 years. They have also been extensively studied scientifically by anthropologists and biologists. However, despite all the empirical and experimental knowledge, no widely accepted explanation for the development of epidermal ridges on fingers, palms and soles has yet emerged. In this article we argue that fingerprint patterns are created as the result of a buckling instability in the basal cell layer of the fetal epidermis. Analysis of the well-known von Karman equations informs us that the buckling direction is perpendicular to the direction of greatest stress in the basal layer. We propose that this stress is induced by resistance of furrows and creases to the differential growth of the basal layer and regression of the volar pads during the time of ridge formation. These ideas have been tested by computer experiments. The results are in close harmony with observations. Specifically, they are consistent with the well-known observation that the pattern type is related to the geometry of the fingertip surface when fingerprint patterns are formed.

© 2005 Elsevier Ltd. All rights reserved.

PACS: 87.18.La; 87.19.Rr

Keywords: Fingerprints; Epidermal ridges; Morphogenesis; Mathematical model

1. Introduction

The pattern of the epidermal ridges on our fingers, palms and soles, the first colloquially called fingerprints, is part of our every-day life. It is characterized by almost parallel ridges that form distinguishable configurations. On the fingertips three main pattern types are discriminated: whorls, loops and arches (see Fig. 1). Loops occur as ulnar loops (when the loop opens toward the small finger) and radial loops (when the loop opens toward the thumb). These configurations are associated with triradii. A triradius (see Fig. 1 (a)) consists of three ridge systems converging to each other at an angle of roughly 120° . More complex patterns, so-called acci-

dentials, do occur but are relatively rare. Furthermore, the pattern exhibits many defects (usually called minutiae in fingerprint literature) such as dislocations (ridge endings, ridge bifurcations), island ridge and incipient ridges (see Fig. 2). These details have received significant attention by forensic science because they make everybody's fingerprint unique and do not change in life. Other applications of fingerprints include the diagnosis of certain genetic defects and ethnic studies although they seem to become obsolete due to the introduction of DNA methods. See Cummins and Midlo (1976) for more background information.

Fingerprints have been extensively investigated from many points of view. Many detailed studies on their embryogenesis exist, numerous papers have been written on the inheritance of certain fingerprint features and they have been statistically linked to all kinds of common human features (gender) and some more obscure ones (sexual orientation, high blood pressure).

*Corresponding author. Current address: Theoretical Physics II, University of Bayreuth, 95440 Bayreuth, Germany. Tel.: +49 921 553229; fax: +49 921 552991.

E-mail address: michael.kuecken@uni-bayreuth.de (M. Kücken).

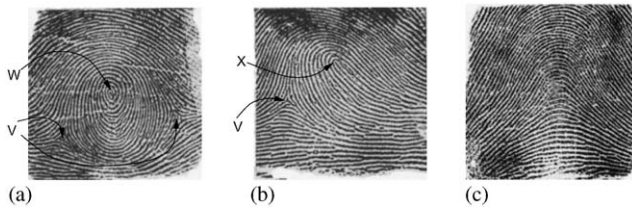


Fig. 1. The most frequently occurring fingertip patterns: (a) whorl, (b) loop and (c) arch. A whorl is characterized by a target/spiral (W) and two triradii (V,V), loops by a Roman arch structure (X) and one triradius (V).

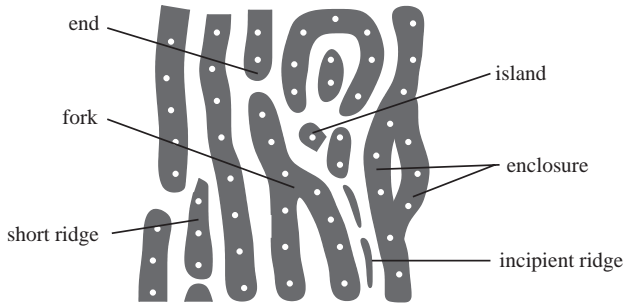


Fig. 2. Examples of minutiae. The white dots represent sweat pores.

In spite of this comprehensive knowledge, to date no commonly accepted mechanism for fingerprint formation exists. Reviewing the literature and existing models, using mathematical modeling and performing computer simulations we will argue in this paper that a mechanical instability is the most likely candidate for the physical process that creates fingerprints. This paper is an extension of the ideas in Kücken and Newell (2004).

2. Biological background

It has been known for a long time that there is a connection between the ridge pattern and anatomical structures, called volar pads (Cummins, 1929). Volar pads are temporary eminences of the volar skin that form at about the 7th week at the fingertips (apical pads), on the distal part of the palm between the digits (interdigital pads) and in the thenar and hypothenar region (thenar and hypothenar pads). The volar pads become less prominent at around the 10th week and then disappear in human embryos.

The crucial events for the establishment of the epidermal ridge pattern take place from the 10th to the 16th week of pregnancy (Babler, 1991; Bonnevie, 1927a; Gould, 1948; Hale, 1951; Hirsch, 1973; Okajima, 1975; Penrose and O'Hara, 1973; Schaeuble, 1932). At the 10th week, embryonal volar skin consists of the layered epidermis on top of the more amorphous fibrous dermis. The innermost layer of the epidermis at the interface to the dermis is called the basal layer and

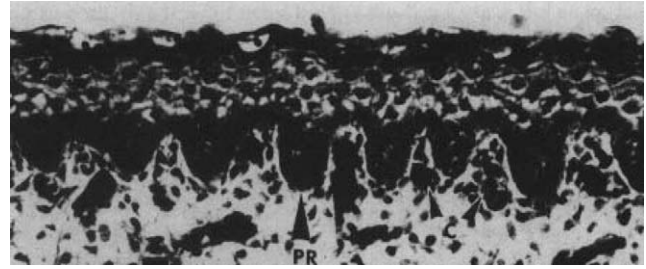


Fig. 3. Undulations in the basal layer appear around the 10th week, become more distinct and form the primary ridges (from Babler (1991)).

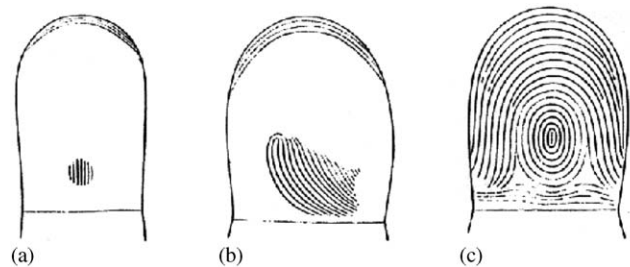


Fig. 4. (a) Ridge formation starts at one or two focal points on the middle of the pad and along the nail furrow. (b) The region where ridges arise first usually coincides with the core of loops or whorls. (c) Ridges spread over the fingertip, the last areas covered by them are the triradii. (from Bonnevie (1927a)).

consists of columnar cells whose axis is perpendicular to the skin surface. It is then observed in embryos of the 10th to 13th week that the basal layer becomes undulated. These undulations quickly become more prominent and form folds of the epidermis into the dermis (see Fig. 3). These folds are called primary ridges. They already establish the future surface pattern, which becomes established at the 16th week. Because fingerprint patterns are encoded at the interface between dermis and epidermis the pattern cannot be destroyed by superficial skin injuries.

Primary ridge formation does not occur simultaneously on the volar surface (Gould, 1948; Bonnevie, 1927a; Schaeuble, 1932). For example, ridge formation on fingers and the palm precedes ridge formation on toes and the sole. Further, ridge formation usually starts at a certain area in the middle of the volar pad (which we will call the ridge anlage) and along the nail furrow; a little later along the interphalangeal flexion crease (see Fig. 4). The area of the ridge anlage usually coincides with the center of whorls and loops if such patterns show up. This way we have three ridge systems on the fingertip (starting from the ridge anlage, the nail furrow and the flexion crease), which slowly spread over the fingertip. At the locations where these ridge systems finally meet, triradii arise.

It is likely from empirical evidence that the primary ridge system changes until the 16th week, when it

becomes permanent (Hale, 1949). For example, it was observed that the number of minutiae significantly rises in that time. A possible reason for this observation could be a larger growth rate of the hand compared to the breadth of the ridges, which would lead to the insertion of new ridges (Hale, 1949).

There are many monkey species where the volar pads do not disappear and persist into adulthood. In these species one often observes whorl structures on very pronounced pads, loops occur on flatter and more lengthy pads whereas regions without pads exhibit almost parallel ridges (Schlaginhaufen, 1905; Whipple, 1904). More evidence for the link between ridge patterns and volar pads comes from studies on human embryos. Babler observed a high percentage of whorls on embryos with early ridge formation (when the pads were still well-developed), only few loops and no arches were found in that case (Babler, 1977). Furthermore, Bonnevie argued that the symmetry of the pad influences the pattern (Bonnevie, 1924, 1929). It can be seen on tables listing the pattern frequencies on different fingers that the only fingers where radial loops occur frequently is finger II (index finger). Ulnar loops are especially frequent on finger V (small finger) whereas whorls are quite common on fingers I (thumb) and IV (ring finger). Bonnevie explained these peculiarities with results of her studies on asymmetries of apical pads. She observed that the pad on finger II is usually slanted toward the small finger, whereas the pad on finger V is slanted toward the thumb. Fingers I and IV were found to be the most symmetric ones (see Fig. 5). Bonnevie explained this observation by the way the fingers separate. According to her, symmetric pads give rise to symmetric patterns like whorls or arches and asymmetric ones give rise to loops. In this situation a pad slanted to the thumb gives rise to an ulnar loop and vice versa.

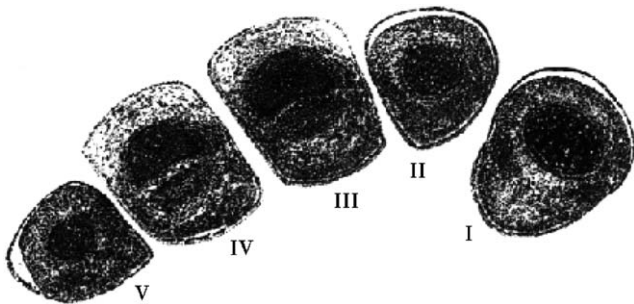


Fig. 5. Cross-sections through the fingertips of the right hand of Bonnevie's embryo No. 83. The thumb is on the right side. The separation of fingers has just occurred and the pads have started to appear. Note that digit I appears fairly symmetric, digit II is slanted slightly to the ulnar direction, digits III and IV are slightly slanted radially and digit V is strongly slanted to the radial side (from Bonnevie (1927a)).

These observations, which were confirmed at observations on malformed hands (Cummins, 1926), provide a strong link between pad geometry and the ridge pattern that develops on them. Both pad bulginess and pad symmetry are important parameter that seem to influence the pattern type. An explanation for this phenomenon has not been found. It is an aim of this paper to bridge this gap.

3. Theories of ridge formation and topological issues

No commonly accepted mechanism for ridge formation exists to date and many contradictory ideas have been published.

Already in 1883 Kollmann speculated that the ridge pattern is established as the result of a folding process, which is induced by differential growth (Kollmann, 1883). With a lot of histological evidence this idea was promoted by Bonnevie in the 1920s. She argued that there is intense cell proliferation in the basal layer of the epidermis resulting in cylindrical cells, which finally evade the stress by folding toward the dermis, thus resulting in the primary ridges (Bonnevie, 1927a, b, 1932). The folding hypothesis was accepted by German researchers of the 1930s (Abel, 1936, 1938; Steffens, 1938) but never convinced the English-speaking fingerprint community. Related to the folding hypothesis is the idea that the ridges form parallel to the largest growth stress as formulated by Cummins (1926). Unfortunately, until now it has never been attempted to identify sources of stress that produce the observed patterns.

Another approach linked the pattern to the nervous system (Dell and Munger, 1986; Moore and Munger, 1989). It is known that the fingertips are innervated before ridge formation starts by a hexagonal pattern of axons whose wavelength roughly equals the one of fingerprints. Arguments against the idea is the fact that a hexagonal planform cannot establish a ridge direction and ridge formation has still been observed in experiments where innervation was prevented (Morohunfola et al., 1992).

Due to similar topological properties of fingerprint patterns and cultivated fibroblast cell patterns it has been suggested that fingerprints are induced by a prepattern in the dermis. On the basis of mechanical interactions between extracellular matrix, haptotaxis and other processes a model was developed (Bentil, 1990; Bentil and Murray, 1993), which, while useful in other contexts, does not seem relevant for understanding fingerprint formation.

Much mathematical research on fingerprints has focused on their topological properties. It has been known for some time that loops and triradii and composites thereof such as whorls and dislocations are

the canonical singularities of two-dimensional stripe patterns in translationally and rotationally invariant systems (Passot and Newell, 1994). These singularities are characterized by a quantity called twist. The twist is defined as the anticlockwise angular rotation of a local wavelike director field whose direction is perpendicular to the ridge crest and whose amplitude is $2\pi/\lambda$ where λ is the local wavelength. The twist around a loop singularity (convex disclination) is π and the twist around a triradius (concave disclination) is $-\pi$. By counting the twist along the margin of the hand in two ways, Penrose found a formula relating the number of loops L , the number of triradii T and the number of digits D in a simple formula ($L + D = T + 1$) (Penrose, 1965, 1979).

Penrose also attempted to explain the observation that there is a relation between pattern type and pad geometry (Penrose and O'Hara, 1973). He thought that the ridges always follow the lines of largest curvature. However, there are a number of exceptions to the rule and no reason is apparent why the ridges should follow the lines of largest curvature. However, his conclusion that ridge direction is determined by a tensor field is consistent with the observation that a pattern containing disclinations (loops and triradii) can only be described by an order parameter which is a director field (equivalent to a tensor field or to a vector field on the double cover of the plane).

4. The model and a little analysis

The folding hypothesis of Kollmann and Bonnevie was the foundation of our modeling approach. We chose it because

- it is the hypothesis best supported by the observations,
- it leads to primary ridges in a very straight-forward way,
- it gives us the right concepts (curvature and forces) to understand the observed relation between pad geometry and ridge direction.

The cytoskeleton of the basal layer cells are attached to each other by desmosomes and to the basal lamina (a seal between dermis and epidermis) by hemidesmosomes. Therefore we can consider the basal layer as an overdamped elastic sheet trapped between the neighboring tissues of the intermediate epidermis layer and the dermis, which we model as beds of weakly nonlinear springs (see Fig. 6). Due to differential growth of the sheet and the constraints of the neighboring layers and boundaries a compressive stress is induced in the sheet. If the compressive stress is large enough, a buckling instability takes place. The balance between the bending resistance of the basal layer and the restoring forces of

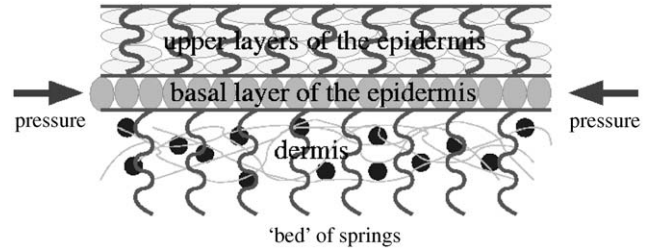


Fig. 6. We consider the basal layer of the epidermis trapped between the intermediate layer and the dermis. Due to differential growth a compressive stress acts on the basal layer.

the elastic foundations establishes a finite wavelength. We analyse this buckling process by minimizing the total elastic energy of the system given by (see Gould, 1999; Kücken, 2004 for details)

$$\mathcal{E} = \int_A \left(\frac{D}{2} (\nabla^2 w)^2 - \frac{1}{2Eh} (\nabla^2 F)^2 + \frac{F_{yy} w}{R_x} + \frac{F_{xx} w}{R_y} - w[F, w] + V(w) \right) dx dy. \quad (1)$$

In this expression F_{yy} denote the second partial derivative of F with respect to y . Further ∇^2 denotes the Laplacian. Also, we assume that the coordinate lines are the lines of principal curvature. The variable w denotes the normal deflection of the sheet and F the Airy stress function. E and $D = \frac{Eh^3}{12(1-\mu^2)}$ are Young's modulus and the bending modulus, respectively. μ is Poisson's ratio. Further h denotes the shell thickness and R_x and R_y are the principal radii of curvature. The bracket is defined as follows:

$$[F, w] = F_{xx} w_{yy} + F_{yy} w_{xx} - 2F_{xy} w_{xy}. \quad (2)$$

Further,

$$V(w) = pw + \frac{cw^2}{2} + \frac{a}{3} w^3 + \frac{b}{4} w^4 \quad (3)$$

is a potential for the resistance of the surrounding tissues to normal displacements. In this expression, p denotes the normal pressure on the sheet, c and b are the linear and cubic spring constant for the elastic foundation (dermis and intermediate layer) and a measures the asymmetry between the forces applied by the two foundations.

The energy contains terms due to bending, in-plane deformations, normal pressure and normal spring resistance. Its functional derivatives give rise to a nonlinear version of the well-known von Karman equations for curved surfaces (Gould, 1999).

$$\kappa w_t + D \nabla^4 w + \frac{F_{yy}}{R_x} + \frac{F_{xx}}{R_y} - [F, w] + V'(w) = 0, \quad (4)$$

$$\frac{1}{Eh} \nabla^4 F - \frac{w_{yy}}{R_x} - \frac{w_{xx}}{R_y} + \frac{1}{2} [w, w] = 0. \quad (5)$$

Here ∇^4 denotes the Bilaplacian.

The analysis that follows is not intended as an exhaustive treatise on the behavior of Eqs. (4) and (5). Rather, it will guide our thinking on fingerprint development and will be used in performing the numerical simulations described in Section 6. In that section, we first calculate a global stress distribution due to the various influences of normal pressure, differential growth and resistance to expansion of the basal layer at boundaries like the nail furrow and flexion creases. Then Eqs. (4) and (5) will be used to find the buckling pattern.

Here we examine what happens to a patch of epidermal skin modeled by an elastic sheet that is compressed by stresses (N_x, N_y) along its principal axes of largest stress. The Airy stress function will then be given by

$$F_0 = \frac{1}{2}N_x y^2 + \frac{1}{2}N_y x^2 \quad (6)$$

and w_0 is the constant solution of

$$V'(w_0) + \frac{N_x}{R_x} + \frac{N_y}{R_y} = 0. \quad (7)$$

If Eq. (7) has more than one solution, we take the lowest amplitude branch. To connote that the stress is compressive we write $N_x = -N$ and $N_y = -\chi N$ where $\chi \leq 1$, meaning that the compression along the x -direction is greater than or equal to the stress along the y -direction. We also take the stress N to be supercritical so that the solution (6), (7) is unstable. To chart the behavior of the buckled surface, we substitute $F = F_0 + f$, $w = w_0 + w'$ into Eqs. (4),(5). Expanding $V'(w_0 + w')$ in a Taylor series and keeping terms to cubic order, we obtain

$$\begin{aligned} \kappa w'_t + D\nabla^4 w' + \frac{1}{R_y} f_{xx} + \frac{1}{R_x} f_{yy} - [f, w'] + Nw'_{xx} \\ + \chi Nw'_{yy} + \gamma w' + \alpha w'^2 + \beta w'^3 = 0 \end{aligned} \quad (8)$$

and

$$\frac{1}{Eh} \nabla^4 f - \frac{1}{R_y} w'_{xx} - \frac{1}{R_x} w'_{yy} + \frac{1}{2}[w', w'] = 0. \quad (9)$$

In these equations we set $V''(w_0) = \gamma$, $\frac{1}{2}V'''(w_0) = \alpha$ and $\frac{1}{6}V^{(4)}(w_0) = \beta$. We examine the linear stability of the (F_0, w_0) solution by ignoring nonlinear terms and setting

$$w(x, y, t) = \widehat{w}e^{\sigma t + i\vec{k}\cdot\vec{x}}, \quad f(x, y, t) = \widehat{f}e^{\sigma t + i\vec{k}\cdot\vec{x}},$$

where $\vec{k} = (l, m)$, $\vec{x} = (x, y)$. Substitute and find the growth rate $\sigma(l, m)$, which is given by

$$\begin{aligned} \kappa\sigma(l, m) = -D(l^2 + m^2)^2 + Nl^2 + \chi Nm^2 \\ - \gamma - \frac{Eh}{(l^2 + m^2)^2} \left(\frac{l^2}{R_y} + \frac{m^2}{R_x} \right)^2. \end{aligned}$$

For $R_x \simeq R_y$, this means that, as N is increased, σ first becomes positive for $\vec{k} = (l_c, 0)$ where

$$l_c^4 = \frac{\gamma}{D} + \frac{12(1 - \mu^2)}{R_y^2 h^2} \quad (10)$$

at a stress value N_c of

$$N_c = D l_c^2 + \frac{\gamma}{l_c^2} + \frac{Eh}{l_c^2 R_y^2}. \quad (11)$$

We can estimate the second term in Eq. (10). From measurements on embryos (Bonnievie's Embryo No. 6 (Bonnievie, 1927a)) we use $R_y = 780 \mu\text{m}$ and $h = 8.0 \mu\text{m}$. Based on the second term, the crest to crest wavelength $2\pi/l_c$ would be about $280 \mu\text{m}$, which is almost nine times larger than the observed value of $36 \mu\text{m}$. Therefore we conclude that the curvature of the epidermal skin surface is much less important than the effect produced by the forces the basal layer feels from its neighboring tissues. We can also estimate the magnitude of γ . It is roughly $D(\frac{2\pi}{36 \mu\text{m}})^4$ or about $10^{-3}(\mu\text{m})^{-4}D$. The fact that curvature is not dominant in choosing the wavelength is consistent with what we observe. The wavelength near the fetal volar pads is approximately the wavelength observed on flat parts of the palm.

We now ask what happens after the instability has taken place. The simplest scenario is a ridge (roll) configuration with the shape

$$w_1(x, y, t) = A_1(t)e^{-il_c x} + A_1^*(t)e^{il_c x}, \quad (12)$$

which grows in amplitude until saturated by the hard springs of the foundation. In our situation this usually happens, although there are exceptions. Another possible scenario is given by a wave triad $w^* = w_1 + w_2 + w_3$ where

$$w_2(x, y, t) = A_2(t)e^{i\frac{l_c}{2}x + iMy} + A_2^*(t)e^{-i\frac{l_c}{2}x - iMy} \quad (13)$$

and

$$w_3(x, y, t) = A_3(t)e^{i\frac{l_c}{2}x - iMy} + A_3^*(t)e^{-i\frac{l_c}{2}x + iMy} \quad (14)$$

for some choice of M . This solution corresponds to a dot (hexagon) pattern. An obstruction to ridge configurations that favors dots arises from the quadratic terms in Eqs. (4) and (5). For example, note that the products $w_2 w_3$, $w_3 w_1$ and $w_1 w_2$, which occur in αw^2 contain some of the same exponential functions that are found in w_1 , w_2 , w_3 . Thus the growths of the amplitudes $A_1(t)$, $A_2(t)$, $A_3(t)$ are affected by products $A_2^* A_3^*$, $A_1^* A_3^*$ and $A_1^* A_2^*$ respectively. Standard analysis (Lange and Newell, 1971, 1974; Kücken, 2004) of the behavior of the system (4), (5) near the bifurcation point $N = N_c$, $\vec{k} = \vec{k}_c$ leads

to the amplitude equations

$$\begin{aligned}\frac{dA_1}{dT} &= \sigma_1 A_1 + \tau A_2^* A_3^* - 3\beta A_1 (|A_1|^2 + 2|A_2|^2 + 2|A_3|^2), \\ \frac{dA_2}{dT} &= \sigma_2 A_2 + \tau A_1^* A_3^* - 3\beta A_2 (2|A_1|^2 + |A_2|^2 + 2|A_3|^2), \\ \frac{dA_3}{dT} &= \sigma_2 A_3 + \tau A_1^* A_2^* - 3\beta A_3 (2|A_1|^2 \\ &\quad + 2|A_2|^2 + |A_3|^2),\end{aligned}\quad (15)$$

where $\sigma_1 = \sigma(l_c, 0)$, $\sigma_2 = \sigma(\frac{l_c}{2}, M) = \sigma(-\frac{l_c}{2}, M)$ and τ is a real constant proportional to α when curvature effects are ignored.

A little calculation shows that solution $A_1 = \sqrt{\frac{\sigma_1}{3\beta}}$, $A_2 = A_3 = 0$ corresponding to ridges whose crests run perpendicular to the directions of greatest stress is stable if

$$\sigma_1 > \frac{\tau^2}{3\beta(2 - \frac{\sigma_2}{\sigma_1})}. \quad (16)$$

Hence, if τ is small and the stress anisotropy large, ridges are favored. On the other hand, when the principal stresses are equal ($\chi = 1$), the choice of wavevectors $l_c(1, 0)$, $l_c(-\frac{1}{2}, \frac{\sqrt{3}}{2})$, $l_c(-\frac{1}{2}, -\frac{\sqrt{3}}{2})$ leads to $\sigma_1 = \sigma_2 = \sigma$. Then, close enough to onset (namely σ small), the stability criterion is

$$\sigma < \frac{4\tau^2}{3\beta}. \quad (17)$$

It can be shown that the stability domain for dot (hexagon) reduces greatly if the stress becomes slightly anisotropic ($\chi < 1$) and vanishes for large anisotropies. Therefore, if the principal stresses are almost equal and the elastic foundation is such that $V'''(w_0) \neq 0$ hexagons are the preferred pattern type for values of the compressive stress close to threshold.

Dot patterns are in fact observed on the dermal surface of certain marsupials such as the vulpine phalanger and the koala. In the koala hexagons are common in flat, featureless areas of the palm (in which an isotropic stress would not be unreasonable) whereas ridges occur parallel to the nail where we (as will be argued later) expect large stress anisotropies (see Fig. 7).

Finally, we estimate the various parameters which arise in our model. From measurements at embryos we will use the following values for the wavelength λ , the wavenumber $k = 2\pi/\lambda$, the shell thickness h and the ridge depth d :

$$\lambda = 36 \mu\text{m}, \quad k = 0.171 / \mu\text{m}, \quad h = 8.0 \mu\text{m}, \quad d = 2 \mu\text{m}.$$

For the ridge depth we point out that we model the situation when the primary ridges have just been created as shallow undulations but have not yet reached their final depth.

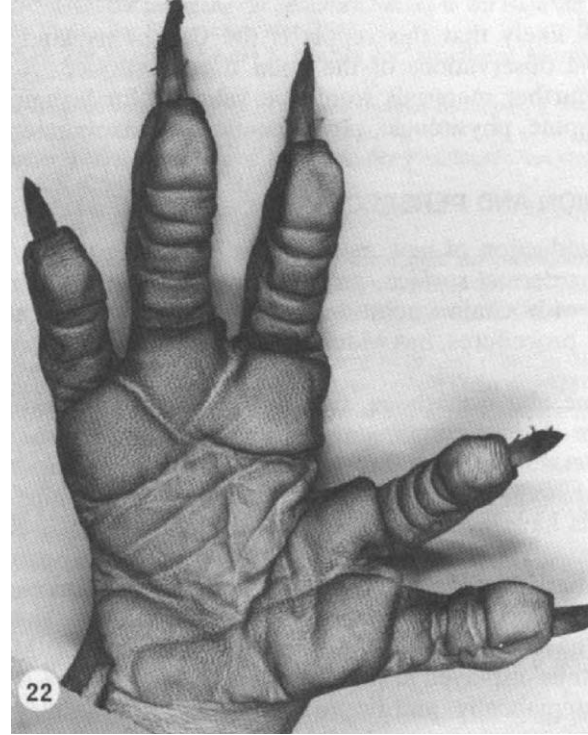


Fig. 7. The dermal surface of a koala. Spots are observed on the palm and ridges form on the finger apex along the nail furrow (from Okajima, 1991).

To continue, we need some estimate of Young's modulus E . As we have pointed out, no real measurements are available, but we can compare the basal layer to tissues where Young's modulus has been measured. Adult skin, however, is not a very suitable comparison object. Its properties are mostly characterized by keratin proteins that are not expressed at primary ridge formation. Furthermore, it seems likely that the mechanical properties of skin are more determined by the keratin rich outer layers than by the basal layer.

For a more reasonable estimate we should look at other epithelial tissues like liver, brain, bladder which all have a Young's modulus in the range from 1 to 100 kPa (Parker et al., 1990). This is much smaller than Young's modulus of materials like steel (2×10^5 MPa) or rubber (7 MPa for small strains). In the following, we will therefore use an estimate of

$$E = 10 \text{ kPa} = 10^{-8} \text{ N}/(\mu\text{m})^2.$$

Poisson's ratio in physical materials ranges from 0 (fully compressible) to 0.5 (incompressible). In our equations, μ only appears in the bending modulus D via the expression $1 - \mu^2$. For the possible ranges of μ this expression can only vary from 0.75 to 1, which is not very much. We estimate Poisson's ratio as

$$\mu = 0.45.$$

From these elasticity constants we determine the bending modulus,

$$D = \frac{Eh^3}{12(1-\mu^2)} = 1.3 \times 10^{-7} \text{ N}\mu\text{m}.$$

Now we can use Eqs. (11) to find the critical stress, N_c , and the linear foundation constant, γ ,

$$N_c = 2k^2D = 7.9 \times 10^{-9} \text{ N}/\mu\text{m},$$

$$\gamma = k^4D = 1.2 \times 10^{-10} \text{ N}/(\mu\text{m})^3.$$

Next we can find an estimate for the cubic foundation term, β , using the ridge depth d ; we find, from the amplitude equations, the relation

$$\frac{d}{2} = \sqrt{\frac{2\gamma\chi}{3\beta}}.$$

Solving for β yields

$$\beta = \frac{8\gamma\chi}{3d^2} \approx 1.6 \times 10^{-11} \text{ N}/(\mu\text{m})^5.$$

In the simulations in this paper we used $\alpha = 0$. Non-vanishing, but small values of α do not seem to influence the buckling patterns.

5. Formation of growth stress

An important result of the previous section was the conclusion that the buckling process is governed by the stresses, not by the curvatures (which, of course, could influence the stress distribution). This implies that the ridges will form perpendicular to the direction of largest stress. Therefore, it is imperative to know how stress is generated in the basal layer.

We believe that the combination of the following two effects is most important:

5.1. Boundary effects

These effects are important to understand why the ridge direction in certain areas is almost always the same in different humans. To understand the basic idea refer to your own hand. Notice the major palm flexion creases, the wrist crease, the phalangeal creases and the nail furrow and observe that the ridges run parallel to these lines. In other words,

the ridges tend to align themselves parallel to the creases and furrows.

Of course, this is only true for the creases that arise prior to ridge formation and not for the ones that form later. At this point, we do not have embryological confirmation that the wrist crease is formed before ridges do. This, however, is clearly true for the other creases mentioned and the nail furrow (Schaeuble, 1932).

Further, notice that there is a relation between ridge direction and the margin of your palm. We see that *the ridges usually arrive at a steep angle at the periphery of the volar surface.*

This angle is often very close to a right angle and almost never less than 45° .

There are a few minor exceptions of these two observations if the ridges are subject to conflicting requirements and some kind of compromise has to be found.

The conclusions of the previous chapter provide us with a framework to understand these observations. Remember, that we consider an expanding cell sheet in which compressive stress is generated due to *resistance* of the surrounding structures. It is likely that the nail furrow and the flexion creases prevent tangential expansion, whereas the margin of the palm may not (or only to a lesser degree). As the basal layer cannot expand toward the creases it will be subjected to compressive forces acting perpendicular to the creases. Since the ridges align themselves along the lines of smallest stress, they will form along the creases, as it is actually observed. The situation is exactly opposite at the margin of the palm. Because basal layer expansion is not resisted here, there are no forces perpendicular to the margin of the palm. This is clearly the direction of smallest stress. Hence, the ridges will align perpendicular to the palm periphery.

As the anatomical position of the flexion creases and the nail furrow in humans is usually very similar, the forces induced by boundary effects are also similar among humans. This explains why the ridge direction is similar in certain regions for almost all people. However, boundary effects do not account for the more individual configurations. The next mechanism aims to explain how the stress field is determined in these regions.

5.2. Normal displacements due to the regression of the volar pads induce tangential stress. This effect is most pronounced close to the ridge anlage

It is well-known that normal displacements of curved surfaces induce in-plane stress if tangential displacements are prevented. The induced stress is compressive if the displacement occurs toward the center of the curvature circle. As we increase the curvature, the compressive stress increases as well. Therefore, normal displacements could possibly explain the observed connection between skin geometry and the stress field that determines ridge direction. But do we actually have normal displacements in the fetal skin when the primary ridges develop?

Primary ridge formation starts at a time when the volar pads regress and become less prominent. Therefore, the assumption that normal displacements create

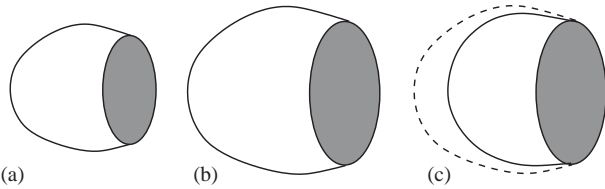


Fig. 8. (a) A cross-section through the apical volar pad at the beginning of volar pad digression. (b) If the fingertip grew exactly uniformly the fingertip would preserve its shape and only increase in size. (c) The fingertip changes its shape due to volar pad regression. The growth forces induced by the regression are obtained by morphing figure (b) into figure (c). To accomplish this task normal displacements toward the center of the pad are necessary.

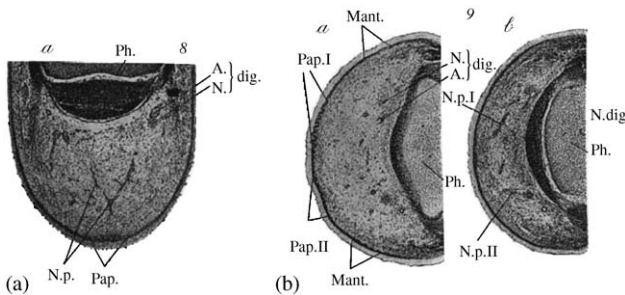


Fig. 9. (a) A cross-section through an embryonic fingertip. The two papillary nerves (*N.p.*) converge towards the ridge anlage (*Pap.*) (from Bonnevie (1927a)). (b) Two cross-sections through an embryonic fingertip. The left figure reveals that two ridge anlagen are present. A more proximal cut shows incomplete convergence of the papillary nerves (*N.p. I* and *N.p. II*) that point to the centers of the ridge anlagen (*Pap. I* and *Pap. II*) (from Bonnevie (1927a)).

tangential stress is very reasonable. However, we have to take into account that the finger as a whole is actually growing at the time of pad digression. Even in this case, our argument is still valid. If all parts of the embryo finger grew at exactly the same rate, the finger would increase its size but exactly preserve its shape. No growth forces are induced in that case. In contrast, changes in the shape of the growing finger will induce forces. These forces can be deduced by relating the finger shape after pad regression to the original finger shape before pad regression (see Fig. 8).

Looking at several of Bonnevie's pictures of cross-sections through fetal fingertip pads (like in Fig. 9(b)) we notice that the usually nicely rounded outline of the pad often becomes flat or even slightly concave at the ridge anlage. Strangely, almost nobody has given this phenomenon much attention. Bonnevie attributed it to the fact that buckling has taken place and the stress is relieved. However, this argument does not explain the degree of concavity found in some specimens. Bonnevie's observations have been confirmed by Schaeuble (1932) at the ridge anlagen of the interdigital pads and more recently by Moore and Munger (1989).

This change in concavity at the ridge anlage indicates that the normal displacements are especially large in that

area. Indeed, it seems as if the epidermis is pulled in by some force here. We may even speculate about the probable origin of this force. The main clue is provided by Fig. 9(a) and (b) which show the papillary nerve projecting to the ridge anlage. It is plausible that the presence of the nerve induces forces that pull in the epidermis. For instance, the nerve could absorb fluids and create an underpressure in the volar pad below the ridge anlage. In fact, this fluid absorption could possibly be the very mechanism for pad digression. If this interpretation is true it would mean that the position of the ridge anlage is indeed caused by the incoming papillary nerves and confirm the importance of the nervous system on the development of epidermal ridges.

These two effects were studied by computer simulations. Furthermore heuristic arguments (Kücken, 2004) establish the link between pad geometry and pattern type.

6. Computer simulations

To test the ideas discussed in this work, a computer program was written that simulates the conditions that we assume are present when fingerprint formation takes place. We show that our results are consistent with the empirical observations and produce the three common configuration types.

In the simulations we proceeded in two steps. At first, we determined how different forces, growth rates and geometries produce a certain stress field. The shape of the prebuckled surface is chosen so as to have enough flexibility to mimic the spectrum of finger shapes. Roughly, it has the form of a half hemisphere sitting on top of a half cylinder but we endow the analytical formula for the surface with enough parameters (16; 17 if we include the cylinder radius) in order to capture as many features as possible and in particular those associated with strongly and weakly swollen volar pads. Because of the non-trivial geometry, the prebuckling stress field is calculated by a finite element algorithm. We will see that the stress field anticipates the buckling pattern in that the direction of smaller principal stress is everywhere the same as the direction of the buckling ridge at that point.

Second, we used the stress field that was obtained in the first step as input to the overdamped von Karman equations; the solutions of which, obtained by spectral methods, then describe what happens after the compressed epidermis buckles. More information is given in Appendix A.

6.1. Finding the stress field

The stress field was obtained using a shell with a fingertip geometry. Different geometries (high pad/low

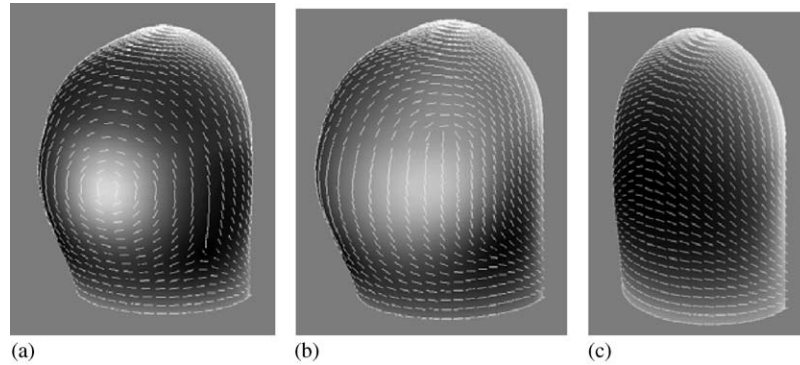


Fig. 10. Boundary forces and normal load produce stress a stress field that, in many aspects, anticipates the future ridge pattern. Here the direction of smallest stress is given (predicting the buckling direction). The color denotes the magnitude of largest compressive stress (white—large compressive stress, black—small compressive stress) and predicts the regions where ridge formation takes place first.

pad, symmetric pad/asymmetric pad) were considered. On this shell the following forces were applied:

- Boundary forces (due to expansion of the basal layer which is resisted at the boundary) perpendicular to the nail furrow and the digital interphalangeal crease compressing the shell.
- Normal load concentrated at the ridge anlage leading to normal displacements.
- Normal and tangential springs.

The boundary forces and the normal and tangential spring constants were the same for all the examples presented here. The normal load and the geometry, however, were varied. The direction of the boundary forces is pointed inwards. Their magnitude is maximal in the spherical part of the fingertip (corresponding to the nail furrow) and decreases along the cylindrical part going down. The forces acting on the bottom (corresponding to the interphalangeal crease) are smaller than those applied to the spherical part.

In Fig. 10 we give examples for the most frequently occurring fingerprint patterns. In these figures the direction field points in the direction of smallest stress, thereby predicting the ridge direction. The color provides the magnitude of the largest principal stress (small stress—black, large stress—white) and therefore predicts in what region fingerprint formation takes place first.

Whorl

The pad is highly rounded and a lot of normal load is applied at the summit of the pad. The stress pattern predicts a whorl, the largest stress is found around the center of the whorl and at the periphery. See Fig. 10(a).

Loop

The pad is strongly slanted to the left-hand side and the center of largest normal load is shifted to the right

side. The normal load is not as concentrated as in the case of a whorl. A loop pattern arises, the loop opens to the right-hand side. The largest stress occurs at the periphery and close to the loop core. See Fig. 10(b).

Arch

The pad is flat and symmetric. Small normal pressure acts on the pad. The normal load is uniform over the fingertip and very small. The stress pattern predicts an arch. Largest stress is found at the periphery. See Fig. 10(c).

Both the connection between pad geometry and configuration type and the predicted timing on ridge spread is in perfect agreement with the descriptions of Bonnevie and others.

6.2. Finding the buckling pattern

We are going to approach the problem by taking the stress field obtained by the finite element program and use it to parameterize the von Karman equations where we dropped the curvature terms. Inevitably, this process has the disadvantage that the stress distribution that was obtained on the curved surface has to be projected into the plane. However these distortions are acceptable because the ridge wavelength is so much smaller than the radii of curvature.

Generally we expect that the ridge lines form perpendicular to the lines of greatest stress. Therefore we anticipate that the direction of the ridge pattern will be given by the stress field. Deviations from this picture are likely to occur especially in areas like centers of whorls, loops or triradii where the ratio of the principal stresses is close to 1. Away from the singularities the ratio of the principal stresses is significantly smaller than 1 (about 0.6–0.8 in most regions on the pad and very low close to the boundary). Therefore, triads are damped and ridges are the favored pattern type.

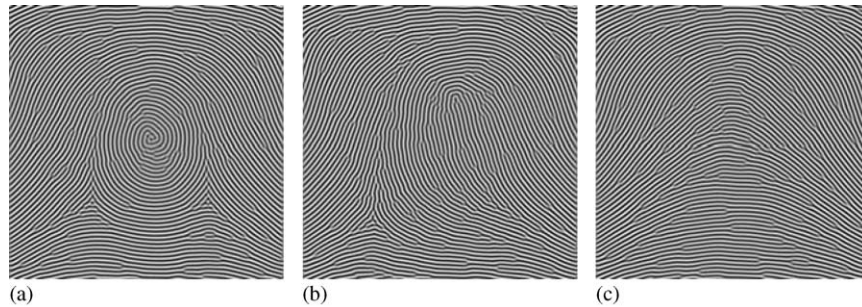


Fig. 11. Simulations of the three common patterns: (a) whorl, (b) loop, (c) arch.

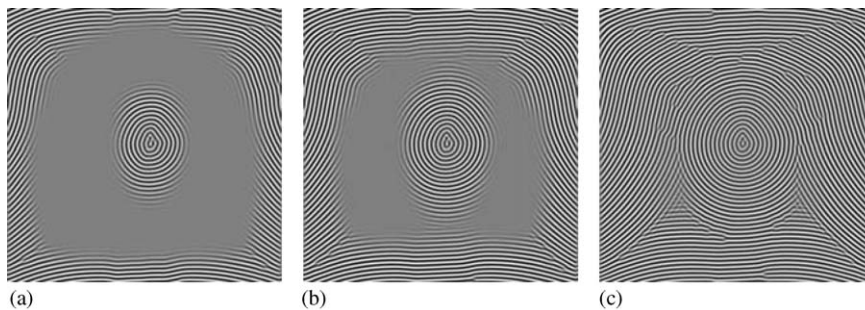


Fig. 12. A whorl pattern forms. The sequence of ridge formation is correct, but the final pattern looks somewhat artificial.

In our simulations we proceeded in the following (somewhat unbiological fashion): At every point the stress field is scaled such that the greatest principal stress is exactly $1.2N_c$. The instability then occurs everywhere simultaneously.

The patterns obtained by this approach (Fig. 11) simulate the general “flow” of fingerprint patterns nicely. Also, the “texture” of dislocations (minutiae) is close to the one we observe in real fingerprints. It is observed that the wavevector is not always exactly parallel to the direction of greatest stress. This especially happens in areas where the ratio of the principal stresses is close to 1. Therefore the wavevector sometimes changes its direction quickly when we follow the ridges from one parallel patch to another. Such a situation can be seen in Fig. 11(a) above the triradii. They rarely occur in real fingerprints. Note also that this phenomenon does not occur above the triradius in Fig. 11(b) where there is a much slower change in the wavevector.

The dislocations (branches and endings) in our simulations mostly occur in two circumstances. They show up when the ridges diverge from each other and new ridges are inserted. Further, they arise in regions where almost parallel ridge patches meet each other (such as the triradii) and the cores of whorls and loops. These are also areas where the ratio of the principal stresses is close to 1. This qualitative observation is consistent with statistics on fingerprint data in forensics (Lee and Gaensslen, 2001) showing that dislocations in

such areas are more frequent than at the periphery. In our simulations we obtained very few dislocations at the periphery, where they are in fact not that rarely observed in real fingerprints. Dislocations at the periphery could arise due to growth of the finger that makes insertion of new ridges necessary. At this point we have not attempted to model such effects.

Changing the initial conditions or parameters slightly does not change the overall pattern type, but results in a distinct change in the placement of the dislocations. In this sense, the dislocations are quite sensitive to their “environment”. This is a reason for the well-observed fact that fingerprints are indeed unique and can be used for identification purposes. This observation is especially important considering the recent challenges of fingerprint permissibility in court and could be a starting point for making the foundations of forensic fingerprint science more credible.

We also generated fingerprints in a slightly different fashion: The complete original stress field is scaled such that it is subcritical everywhere. Then the stress is raised slowly. The instability starts in areas of greatest stress and then slowly spreads over the whole surface. The stress is not raised anymore at a certain point if the critical stress reaches $1.2N_c$.

Although approach 2 does not produce as convincing pictures (see Fig. 12) they are still illuminating and point the way to more realistic models. The sequence of ridge formation—starting at the boundary, the core of loops

and whorls, the spreading over the surface and finally filling in the triradius—is correct. Further the resulting patterns can clearly be recognized as loops and whorls. However, there are some problematic features. The pattern appears very “stiff”, they seem to consist of patches of parallel ridges with discontinuous changes in the wavevector between the patches. Further there are much fewer dislocations, and the ones that arise are distributed in a stereotypical fashion, usually along the patch boundaries.

It is not difficult to locate the reason for these problems. In the course of ridge formation in these simulated patterns the ridges tend to arise adjacent to existing ones. Even if the underlying stress field slightly changes, the wavevector of the existing ridges creates a large enough bias for the new ridges to follow in the same direction (especially if the ratio of the principal stresses is close to 1 and no direction is clearly favored). Patches of parallel ridges arise this way that are not compatible when they meet and the wavevector becomes discontinuous where these patches join each other.

These problems mean that there is certainly more work to do. However, much insight has already been gained, especially concerning the *onset* of buckling. The results we obtained from the linear and weakly-non-linear analysis are consistent with the biological observations and helped us to gain a better understanding how the pattern is laid out. However, in our investigations we limited ourselves to observations that are determined at the instability or shortly after the instability like wavelength, pattern type and ridge direction. We have used very little information about the minutiae and the spread of ridges, in part because little quantitative data is available.

The von Karman equations should be seen as a first model that already captures many important fingerprint features and leaves room for significant improvements. Although buckling is the likely mechanism for the instability that creates fingerprint patterns it cannot explain everything one would like to know about fingerprint development. The buckling model does not tell us much how the ridge system matures from the 10th to the 17th week, however an understanding of this process is crucial for a theory of minutiae.

7. Results and conclusions

We are able to formulate the following hypothesis on the development of epidermal ridges.

The epidermal ridge pattern is established as the result of a buckling instability acting on the basal layer of the epidermis and resulting in the primary ridges.

The buckling process underlying fingerprint development is controlled by the stresses formed in the basal layer, not by the curvatures of the skin surface.

The stresses that determine ridge direction are themselves determined by boundary forces acting at creases and the nail furrow and normal displacements, which are most pronounced close to the ridge anlage. The geometry of the volar pads influences this process.

One way to estimate the quality of our work is to look at Figs. 1 and 11 and compare the real and simulated patterns. They surely have a lot in common, such as the topology, an established wavelength and similar ridge direction. They are different in some respects that are not important because the underlying stress field is somewhat different (for instance the simulated loop appears “higher up” than the real one). And there are some differences that should be the cause of further work such as the behavior in regions of rapid ridge direction change or the stiffness of the simulated pattern in some regions.

Even more important than the resemblance of reality and simulation is the fact that the ideas in this work integrate the mainstream ideas on fingerprints. Our model confirms that:

- Primary ridges are formed as the result of a buckling process.
- Ridges form perpendicular to the lines of greatest stress as postulated.
- Volar pad geometry influences the fingerprint pattern as observed.
- The nervous system is involved this process.
- Although ridges are the usual pattern, dots (hexagons) are another possibility.
- After the buckling instability has taken place and the ridge pattern is established, cell proliferations may increase the depth of the primary ridges.

Further we do not rule out that other biological effects that are reported in the literature influence the postbuckling behavior and form the fingerprint pattern on our fingers, palms and soles, that we see every day. The mathematical techniques provide the means of relating these ideas into a unified whole.

The theory presented provides for the first time a consistent picture how growth and pad geometry produce the observed patterns. It further illuminates the role of curvature, which does not affect the pattern directly through the buckling process but indirectly through the formation of growth stress.

This way our theory provides a basis for any further work. So far our investigations have been focused on the major pattern types; an extension should also encompass more complex patterns such as double-loops or more complex loops. Furthermore, a more sophisticated theory for minutiae is needed that could help to put forensic fingerprint identification on a more profound foundation. Unfortunately the knowledge on the

embryological development of minutiae, imperative for any modelbuilding, is very sparse.

Acknowledgments

We want to thank Patrick Shipman for helpful discussions and valuable comments. This work was partially supported by NSF Grant DMS 0202440.

Appendix A. Numerical algorithms

The method of finite elements has proven to be the method of choice for problems of complex geometries. Because the non-trivial geometry of the finger is essential for fingerprint development finite elements were used to determine the stress field that is formed as the result of certain growth forces.

For our purposes we chose the algorithms described in chapter 8 in Zienkiewicz and Taylor (2000b) and chapter 6 in Hughes (1987). This approach treats shells as three-dimensional body where one dimension (the thickness) is much smaller than the others. The approach does not assume Kirchhoff's hypothesis (normals remain normal after deformation) but the more realistic Reissner–Mindlin assumption (normals remain straight lines but are not necessarily normal anymore) that takes transverse shear phenomena into account and gives good results, even for moderately thick shells. Throughout the calculation we used simple, 4-node, bilinear, quadratic elements.

Boundary conditions can be imposed by modifying the stiffness matrix so that certain values are enforced for boundary displacements. These displacements are prescribed in terms of the local coordinate system. An alternative way of ensuring that the stiffness matrix is non-singular is the attachment of spring forces at some or every node. This is easily implemented by increasing the diagonal elements of the stiffness matrix.

It is well-known that the approximation of the strains and stresses is relatively poor at the nodes itself and much better results can be accomplished by using certain interior points. To avoid this problem the superconvergent patch recovery (SPR) method described in Zienkiewicz and Taylor (2000a) was used. Here the strains are determined at the interior points and the node stresses are recovered by a least square approximation.

The fingertip is constructed as a domain in spherical coordinates (the fingertip) above a domain in cylindrical coordinates. We define the surface as a map from a rectangular region Ω . Let $(u, v) \in \Omega$. Then the surface S is defined as the image of the map $r : \Omega \rightarrow S$. The map is

defined for $v < 0$ as

$$r(u, v) = \begin{pmatrix} \rho(u, v) \cos(u/r_0) \\ v \\ \rho(u, v) \sin(u/r_0) \end{pmatrix}$$

and for $v > 0$ as

$$r(u, v) = \begin{pmatrix} \rho(u, v) \cos(u/r_0) \cos(v/r_0) \\ \rho(u, v) \sin(v/r_0) \\ \rho(u, v) \sin(u/r_0) \cos(v/r_0) \end{pmatrix}.$$

Here r_0 is a parameter that should be chosen close to the average of the radius of pad curvature. Further we have a function $\rho(u, v)$ that denotes the distance of the surface from the y -axis in the cylinder part and the distance from the origin in the spherical part of the surface. This construction ensures a smooth (at least once differentiable) surface for all smooth $\rho(u, v)$.

The pad geometry can now be specified by choosing a certain function $\rho(u, v)$. In our simulations it is given by the following expression

$$\begin{aligned} \rho(u, v) = & [c_1 + (c_2 e^{\frac{(v-c_3)^2}{c_4}} + c_5) \sin(u/r_0) \\ & + (c_6 e^{\frac{(v-c_7)^2}{c_8}} + c_9) \sin(2u/r_0) \\ & + (c_{10} e^{\frac{(v-c_{11})^2}{c_{12}}} + c_{13}) \sin(3u/r_0)] \cdot \theta \\ & + \frac{1}{\sqrt{\frac{\cos^2(v/r_0)}{c_1^2} + \frac{\sin^2(v/r_0)}{c_{14}^2}}} \cdot (1 - \theta), \end{aligned}$$

where

$$\theta = \frac{\tanh(-c_{15}(v - c_{16})) + 1}{2}.$$

Along a horizontal cross-section the function is defined by the first four terms of a sine series in the cylinder part. Along the length of the cylinder, the coefficients of the sine series are varied according to a Gaussian. In the spherical part, a smooth transition into an ellipsoid is achieved. Using this paradigm many different shapes can be obtained, although the many parameters (16!) are certainly a drawback of the method.

The von Karman equations are solved using a simple spectral scheme. As w is updated we used a scheme implicit in all linear terms and explicit in all nonlinear terms. The spectral scheme implies periodic boundary conditions, that are acceptable in this case because the pattern in w is locally determined by the stress tensor, not by the boundary conditions. Slight disturbances at the boundaries are possible, but insignificant.

References

- Abel, W., 1936. Über Störungen der Papillarmuster. Z. Morphol. Anthropol. 36, 1–38.

- Abel, W., 1938. Kritische studien über die entwicklung der papillarmuster auf den fingerbeeren. *Z. Mensch. Vererb. Kons* 21, 497–529.
- Babler, W., 1977. The prenatal origins of populational differences in human dermatoglyphics. Ph.D. Thesis, University of Michigan.
- Babler, W., 1991. Embryologic development of epidermal ridges and their configurations. In: Plato, C., Garruto, R., Schaumann, B. (Eds.), *Dermatoglyphics: Science in Transition*. Wiley-Liss, Inc.
- Bentil, D., 1990. Aspects of dynamic pattern generation in embryology and epidemiology. Ph.D. Thesis, Wolfson College, Oxford.
- Bentil, D., Murray, J., 1993. On the mechanical theory for biological pattern formation. *Physica D* 63, 161–190.
- Bonnevie, K., 1924. Studies on papillary patterns in human fingers. *J. Genet.* 15, 1–111.
- Bonnevie, K., 1927a. Die ersten entwicklungsstadien der papillarmuster der menschlichen fingerballen. *Nyt. Mag. Naturvidenskaberne* 65, 19–56.
- Bonnevie, K., 1927b. Zur mechanik der papillarmusterbildung I. *Roux. Arch. Dev. Biol.* 117, 384–420.
- Bonnevie, K., 1929. Was lehrt die embryologie der papillarmuster über ihre bedeutung als rassen- und familiencharakter, Part I and II. *Z. Indukt. Abstamm. Ver.* 50, 219–274.
- Bonnevie, K., 1932. Zur mechanik der papillarmusterbildung II. *Roux. Arch. Dev. Biol.* 126, 348–372.
- Cummins, H., 1926. Epidermal-ridge configurations in developmental defects, with particular reference to the ontogenetic factors which condition ridge direction. *Am. J. Anat.* 38, 89–151.
- Cummins, H., 1929. The topographic history of the volar pads (walking pads; Tastballen) in the human embryo. *Contrib. Embryol.* 113 (20), 105–126.
- Cummins, H., Midlo, C., 1976. *Finger Prints, Palms and Soles*. Research Publishing Company, Inc.
- Dell, D., Munger, B., 1986. The early embryogenesis of papillary (sweat duct) ridges in primate glabrous skin: the dermatotopic map of cutaneous mechanoreceptors and dermatoglyphics. *J. Comput. Neurol.* 244, 511–532.
- Gould, E., 1948. A topographic study of the differentiation of the dermatoglyphics in the human embryo. Ph.D. Thesis, Tulane University.
- Gould, P., 1999. *Analysis of Plates and Shells*. Prentice-Hall, Englewood Cliffs, NJ.
- Hale, A., 1949. Breadth of epidermal ridges in the human fetus and its relation to the growth of the hand and foot. *Anat. Rec.* 105, 763–776.
- Hale, A., 1951. Morphogenesis of volar skin in the human fetus. *Am. J. Anat.* 91, 147–180.
- Hirsch, W., 1973. Morphological evidence concerning the problem of skin ridge formation. *J. Ment. Defic. Res.* 17, 58–72.
- Hughes, T., 1987. *The Finite Element Method*. Prentice-Hall, Englewood Cliffs, NJ.
- Kollmann, A., 1883. *Der Tastapparat der Menschlichen Rassen und der Affen in Seiner Entwicklung und Gliederung*. Voss Verlag.
- Kücken, M., 2004. On the formation of fingerprints. Ph.D. Thesis, University of Arizona.
- Kücken, M., Newell, A., 2004. A model for fingerprint formation. *Europhys. Lett.* 68, 141–146.
- Lange, C., Newell, A., 1971. The post-buckling problem for thin elastic shells. *SIAM J. Appl. Math.* 605–629.
- Lange, C., Newell, A., 1974. Spherical shells like hexagons. *J. Appl. Mech. Paper No.* 73-APM-7.
- Lee, H., Gaensslen, R., 2001. *Advances in Fingerprint Technology*. CRC Press, Boca Raton.
- Moore, S., Munger, B., 1989. The early ontogeny of the afferent nerves and papillary ridges in human digital glabrous skin. *Dev. Brain Res.* 48, 119–141.
- Morohunfo, K., Jones, T., Munger, B., 1992. The differentiation of the skin and its appendages II. Altered development of papillary ridges following neurolectomy. *Anat. Rec.* 232, 599–611.
- Okajima, M., 1975. Development of dermal ridges in the fetus. *J. Med. Genet.* 12, 243–250.
- Okajima, M., 1991. Nonprimate Mammalian Dermatoglyphics as Models for Genetic and Embryologic Studies: Comparative and Methodologic Aspects. In: Plato, C.C., Garruto, R.M., Schumann, B.D. (Eds.), *Dermatoglyphics: Science in Transition*. Wiley-Liss, Inc., New York.
- Parker, K., Huang, S., Musulin, R., Lerner, R., 1990. Tissue response to mechanical vibrations for “sonoelastic imaging”. *Ultrasound Med. Biol.* 16, 241–246.
- Passot, T., Newell, A., 1994. Towards a universal theory for natural patterns. *Physica D* 74, 301–352.
- Penrose, L., 1965. Dermatoglyphic topology. *Nature* 205, 544–546.
- Penrose, R., 1979. The topology of ridge systems. *Ann. Hum. Genet.* 42, 435–444.
- Penrose, L., O'Hara, P., 1973. The development of epidermal ridges. *J. Med. Genet.* 10, 201–208.
- Schaeuble, J., 1932. Die Entstehung der palmaren Triradien. *Z. Morphol. Anthropol.* 31, 403–438.
- Schlaginhaufen, O., 1905. Das hautleistensystem der primatenplanta unter mitberücksichtigung der palma teil I. *Morphol. Jahrb.* 33, 577–671.
- Steffens, C., 1938. Über zehenleisten bei zwillingen. *Z. Morphol. Anthropol.* 37, 218–258.
- Whipple, I., 1904. The ventral surface of the mammalian chirodium with especial reference to the condition found in man. *Z. Morphol. Anthropol.* 7, 261–368.
- Zienkiewicz, O., Taylor, R., 2000a. *The Finite Element Method, vol. 1: The Basis*. Butterworth Heinemann, London.
- Zienkiewicz, O., Taylor, R., 2000b. *The Finite Element Method, vol. 2: Solid Mechanics*. Butterworth Heinemann, London.